A METHOD FOR CALCULATING AERODYNAMIC HEATING ON

Flight Performance Branch
Sounding Rocket Division
NASA Goddard Space Flight Center

Abstract

A method is presented for calculating the aerodynamic heating and shear stresses at the wall for tangent ogive noses that are slender enough to maintain an attached nose shock through that portion of flight during which heat transfer from the boundary layer to the wall is significant. The lower entropy of the attached nose shock combined with the inclusion of the streamwise pressure gradient yields a reasonable estimate of the actual flow conditions. Both laminar and turbulent boundary layers are examined and an approximation of the effects of (up to) moderate angles-of-attack is included in the analysis. The analytical method has been programmed in Fortran IV for an IBM 360/91 computer.

Symbols

C_f = friction coefficient local (-)

C_p = specific heat of air (Btu/lbm °K)

$(dv/dx)_{(0)}$ = Newtonian velocity gradient at the stagnation point on a circular nose (sec^{-1}) (see Eq. 19)

$f''_{(w)}$ = velocity gradient parameter from Reference (6) (see Eqs. 27 and 28)

g = acceleration of gravity (32.174 ft/sec^2)

h = enthalpy (Btu/lbm)

h^* = reference enthalpy (Btu/lbm)

$H^*_{(0)}$ = defined by Equation (18)

$H^*_{(x)}$ = defined by Equation (17)

k = coefficient of thermal conductivity (Btu/ft sec °K)

N = a constant; set = 0 for one-dimensional flow; set = 1 for axisymmetric flow (= 1 throughout this program)

Nu = Nusselt Number (-)

$P(I)$ = pressure at stations 1 through 15 (atmospheres, except where otherwise noted)

P_r = Prandtl Number (-)

$PXPO(I)$ = the local to stagnation point pressure ratio at each of the 15 station locations (-)

$\dot{q}$ = heat transfer rate (Btu/ft^2 sec)

$QRATL$ = ratio of heat transfer with cross flow to that without cross flow for a laminar boundary layer (see Eq. 29) (-)

$QRATT$ = ratio of heat transfer with cross flow to that without cross flow for a turbulent boundary layer (see Eq. 30) (-)

R = tangent ogive radius of curvature (see Figures 1 and 2) (ft)

R_e or $R_{e(x)}$ = local Reynolds number (Eq. 25) (-)

$R_{e(\theta)}$ = local momentum thickness Reynolds number (Eq. 26) (-)

R_N = spherical nose radius (for calculations of blunt body stagnation point heat transfer rate) (ft)

$r(I)$ or $r(X)$ = the flow deflection distance defined by Eq. (11) and shown in Figures 1 and 2 (ft)

V = velocity (ft/sec)

X = tangent ogive longitudinal dimension (shown in Figures 1 and 2) (ft)

$X(I)$ = surface coordinate distance along streamline from nose tip to each station (ft)

Y = tangent ogive base radius, shown in Figures 1 and 2 (ft)

α = ALPHA = the vehicle angle-of-attack (deg. or rad.)

δ_{cr} = the flow deflection angle (conical flow) at which the nose shock becomes detached for a given free stream Mach number (deg. or rad.)

θ = the local surface deflection angle; also, the central angle turned by the tangent ogive radius, R, to define the complete ogive (see Figures 1 and 2) (deg. or rad.)

θ_c = cone half-angle (deg. or rad.)

μ = viscosity coefficient (lbf sec/ft^2)

ρ = density of air (lbm sec^2/ft^4 = slugs/ft^3)

τ = boundary layer shear stress at the wall (lbf/ft^2)

$\phi(I)$ = angle defined by Eq. (10) and shown in Figure 2 (deg. or rad.)

Subscripts

e = local, external-to-the-boundary layer value

Lam = considers a laminar boundary layer

rec = evaluated at recovery conditions

ref = evaluated at reference conditions (see superscript)

Turb = considers a turbulent boundary layer

x = at a position X feet from nose tip along a surface streamline (same as e)

w = evaluated at local pressure and wall temperature

o = at stagnation point for a spherical nose of Radius, R_N

∞ = free stream (ahead of nose shock) value

Superscript

* = property evaluated at local pressure and reference enthalpy

Introduction

The generally favorable aerodynamic characteristics of the tangent ogive in supersonic and hypersonic flow result in the common use of this configuration for sounding rocket noses. Accordingly, an analytical method for calculating the aerodynamic heating on such configurations has been devised, combining basic analytical methods which are well known with some which are less common and with certain basic assumptions. These methods, while approximate in nature, yield results which have proved to be adequate for the design of both the structure of the rocket nose and the protection of payload items within. The entire analysis described here has been programmed in Fortran IV for an IBM 360/91 system (Reference 1).

The slenderness of the ogives of interest results in an attached nose shock wave through periods of supersonic and hypersonic flight during which significant aerodynamic heating is experienced. The low entropy-jump across the oblique shock wave as opposed to the entropy-jump across the normal shock wave associated with "blunt bodies" results in an increase of heat transfer to the ogive for a constant flight condition. This is similar to the case of the cone heating as compared to that on a blunt, axisymmetric body. However, unlike the cone case, the ogive body has a definite (first order) pressure gradient along the surface streamlines. A blunt body analysis is treated in Reference (2) and a conical body analysis in Reference (3). The present analysis considers the in-between (tangent ogive) case in which the nose shock is oblique but there is a body pressure gradient. The effects of moderate angle-of-attack (local body angle plus angle-of-attack of 30 to 35 degrees) are approximated.

Theory

The theory is derived from a combination of the analytical methods of References (2) and (3) with several new approximations and assumptions. The pertinent geometry along with the most important items of nomenclature are shown in Figures 1 and 2. The tangent ogive and flow geometry are completely defined by the parameters x_{max}, y_{max} and α (identified in Figure 1) in conjunction with the geometric equations (7 through 12). The
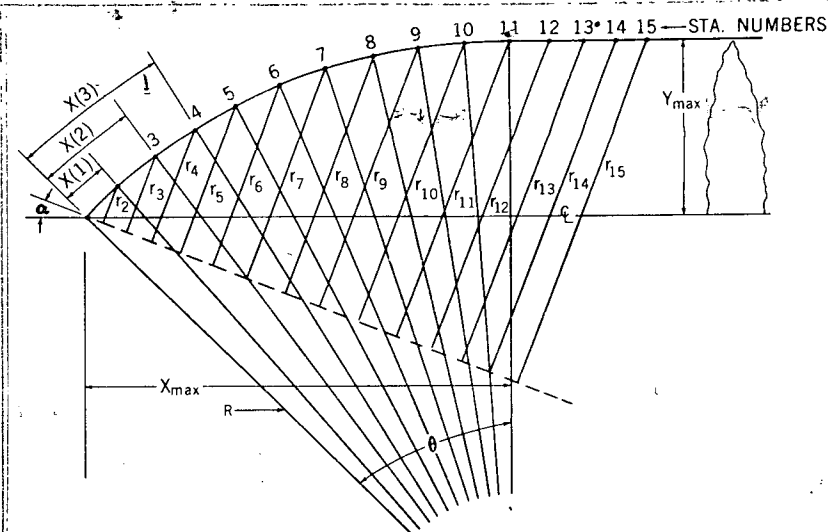

Figure 1. Geometry of Tangent Ogive Nose

effects of (up to) moderate angles-of-attack are accounted for by assuming the local flow to be similar to that on a cone of half-angle (equal to the ogive local surface angle) at angle-of-attack. The applicable free stream conditions are derived either from the vehicle altitude and an appropriate ARDC atmosphere or by electing to define the pre-nose shock air properties by specifying two thermodynamic variables — the pressure and the temperature — then obtaining all the other properties from the real gas (equilibrium) Mollier approximations of Hansen (Reference 4).

For simplicity, a fixed number of body locations are specified for each problem. Either of two procedures can be adopted for defining the local flow conditions at these specified 15 body points. In the first case, the local pressures at the calculation points are defined by Newtonian approximations or from experiment (if available). The entropy behind the attached nose shock (assumed to be conical) is then calculated and the local, external-to-boundary layer properties are defined by isentropically expanding to the given local pressures. This assumes that
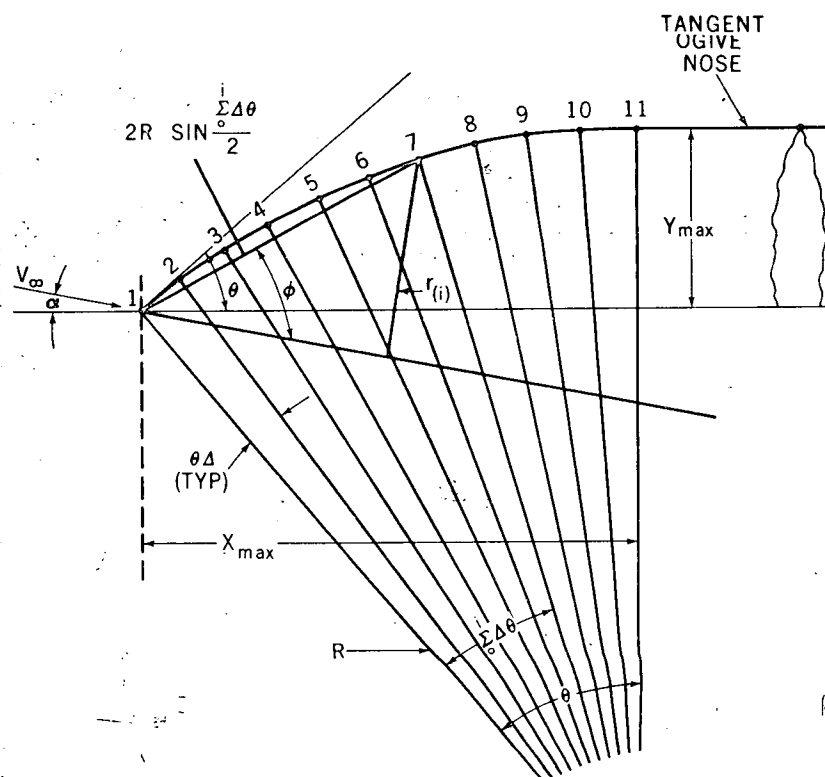

Figure 2. Definitions of Math Symbols

the entropy is constant at the post-nose shock value over the entire body and results in an over-prediction of the available energy, hence, heat transfer rate to the wall. The second method obtains the post-nose shock entropy and pressure (as in the first method) and taking these data as initial values, uses a Prandtl-Meyer expansion through $\Delta\theta$ degrees to get the pressure at point 2 (Figure 1). This pressure and the point 1 entropy are then used with the air properties of Reference (4) to define all external-to-bounday layer properties at point 2. The local surface angle at point 2 is then considered to be the cone half-angle and a new cone (external-to-boundary layer) entropy at point 2 is calculated and used in the same manner as just described to expand by an appropriate Prandtl-Meyer routine through $\Delta\theta$ degrees to obtain the point 3 pressure at the point 2 entropy. In this way, the properties at each point on the ogive are approximated by using the entropy of the immediate upstream point.

This method represents an attempt to approximate the entropy gradient across the shock layer. Note that the entropies so derived are conservatively lower the farther aft one goes on the ogive. Moreover, the greatest conservatism in the predictions of the local heat transfer rate occurs at point 11. For all points downstream of 11, the entropy is left at the point 11 calculated value and the pressures are assumed to be the arithmetic average of the free stream (ahead of the nose shock) and the point just upstream of the point being studied. Mathematically:

$$SR\,(11) = SR\,(12) = SR\,(13) = SR\,(14) = SR\,(15) \quad (1)$$

and

$$P\,(11) = \left(P_\infty + P\,(10)\right)/2 \quad (2)$$

$$P\,(12) = \left(P_\infty + P\,(11)\right)/2 \quad (3)$$

$$P\,(13) = \left(P_\infty + P\,(12)\right)/2 \quad (4)$$

$$P\,(14) = \left(P_\infty + P\,(13)\right)/2 \quad (5)$$

$$P\,(15) = P_\infty \quad (6)$$

Of course, the Prandtl-Meyer expansion is used only up to and including point 11. From point 11 to points 12, 13, 14, and 15, the entropy is constant and isentropic expansion to the local pressures indicated in Equations (2) through (6) defines the local flow properties. The calculated pressure is not allowed to go below 80 percent of the free stream pressure — as would sometimes result from the Prandtl-Meyer expansion technique described.

It should be emphasized that while the entropy values for the second method are low (yielding conservatively high heat transfer rates), the pressures that result from the Prandtl-Meyer expansion technique are also normally on the low side. This tends to decrease the predicted heat transfer rates. The two effects tend to offset each other.

Geometric Calculations

The programming of the analysis is greatly simplified by the fact that a fixed number of stations on a fixed geometry (the tangent ogive followed by a cylinder) are treated. In specifying the magnitude of x_{max} and y_{max} and the angle-of-attack, α, all necessary geometric input has been supplied and one is able to generate the geometric details required by means of the following equations (the nomenclature of which is defined in Figure 2): Given only x_{max}, y_{max} and α

$$R = \frac{x^2 + y^2}{2\,y} \quad (7)$$

$$\theta = \mathrm{Tan}^{-1}\left[\frac{x}{R-y}\right] = \mathrm{Tan}^{-1}\left[\frac{2 \cdot x \cdot y}{x^2 - y^2}\right] \quad (8)$$

$\Delta\theta$ is defined as

$$\Delta\theta = 0.1\,(\theta) \quad (9)$$

In order to calculate the "flow deflection" distance, $r(i)$, define

$$\phi\,(i) = PHI\,(i) = \theta + \alpha - \frac{\sum_0^i \Delta\theta}{2} \quad (10)$$

and thence (from the right triangle of Figure 2)

$$r\,(i) = 2\,R\,\sin\left[\frac{\sum_0^i \Delta\theta}{2}\right]\sin\phi\,(i) \quad (11)$$

The surface coordinate distance (boundary layer build-up distance) is

$$X(i) = R\sum_1^i \Delta\theta_i \quad (12)$$

Assumptions

The following basic assumptions are applicable to the analytical methods:

1. The shock layer entropy gradient effect on the external-to-boundary layer flow properties around the ogive is approximated by assuming the local external flow to have originated just downstream of a shock wave generated by a cone of the same half-angle as the local surface angle $(\theta + \alpha)$. This tends to predict increasingly lower (than the true local value) entropies as one considers points farther downstream on the ogive. The predicted heat transfer, therefore, is expected to become increasingly conservative as the farther downstream stations are treated.

3

2. In the alternate method in which pressures are input and the entropy is constant at the post-nose shock (point 1) value, the calculated entropy is expected to be higher than the actual values for downstream points, again the error growing with distance downstream. Accordingly, lower heat transfer rates downstream should result from the entropy effect of the pressure-input option. Note that one cannot conclude from this that the heat rate distributions from this method are actually conservative because their magnitudes in this option are also highly dependent upon the magnitudes of the pressures that are input. The above remarks refer to the entropy effect alone (as though the pressures by either method were equal).

3. It is assumed that the increase in heat transfer rate caused by the thinning of the boundary layer (resulting from the cross flow) at any station on the ogive nose can be approximated by the use of Equations (29) and (30), substituting the local surface angle (θ) for the cone half-angle, θ_c. The validity of this local similarity assumption has not been established independently at this writing.

Heat Transfer Rate and Shear Stress on Body

The boundary layer heat transfer rate and shear stresses at the wall are calculated by means of (a) the Eckert and Tewfik adaptation of Lee's momentum integral equation (Reference 5) and the use of Reynolds analogy for the laminar case, and (b) the Flat Plate Reference Enthalpy Method described in Reference (6) (also applying Reynolds analogy) for the turbulent boundary layer case. The programmed equations are:

1. Laminar heat rate (ratioed to the spherical nose stagnation point heat rate) (Reference 5)

$$\frac{\dot{q}(x)}{\dot{q}(0)} = \left[\frac{k^*_{(x)}}{k^*_{(0)}}\right]\left[\frac{H^*_{(x)}}{H^*_{(0)}}\right]\left[\frac{h_{rec} - h_{(w)}}{h_{(0)} - h_{(w)}}\right]\left[\frac{C_{P_{w(0)}}}{C_{P_{w(x)}}}\right] \quad (13)$$

where the starred quantities are evaluated at local pressure and reference enthalpy, h^*.

$$h^* = h_{ref} = \frac{h_{(e)} + h_{(w)}}{2} + 0.22\sqrt{\rho_{r_{(e)}}}(h_{(0)} - h_{(w)}) \quad (14)$$

$$h_{rec} = h_{(e)}\left[1 - (p^*_r)^{1/2} + h_{(0)}(\rho^*_r)^{1/2}\right]_{(Laminar\,B.L.)} \quad (15)$$

or

$$h_{rec} = h_{(e)}\left[1 - (p^*_r)^{1/3} + h_{(0)}(p^*_r)^{1/3}\right]_{(Turbulent\,B.L.)} \quad (16)$$

In Equation (13), H*(x) is given by:

$$H^*_{(x)} = \left[\frac{\rho^*_{(x)}}{\rho^*_{(0)}}\right]\left[\frac{V_{(x)}}{V_{(0)}}\right](r(x))^N \left\{\int_0^x \left[\frac{\rho^*_{(x)}\,\mu^*_{(x)}}{\rho^*_{(0)}\,\mu^*_{(0)}}\right]\left[\frac{V_{(x)}}{V_{(\infty)}}\right](r(x))^{2N}\,dx\right\}^{1/2} \quad (17)$$

N = 0 for two-dimensional and N = 1 for axisymmetric flow (hence N = 1 for the case considered) and

$$H^*_{(0)} = \left[\frac{\frac{2\,\rho^*_{(x)}}{\rho^*_{(0)}}\left(\frac{dV}{dx}\right)_0}{V_\infty(\mu^*_{(x)}/\mu^*_{(0)})}\right]^{1/2}(1+N)^{1/2} \quad (18)$$

is the stagnation point value.

Note that $(dv/dx)_{(0)}$ is given the Newtonian (circular nose) value

$$\left(\frac{dV}{dx}\right)_0 = \frac{\sqrt{2}}{R_n}\left[\frac{P_{(0)} - P_{(\infty)}}{\rho_{(0)}}\right]^{1/2} \quad (19)$$

The turbulent heating equation is (Reference 6):

$$\dot{q}_{Turb} = \frac{0.03(g)^{1/3}(1+N)^{\cdot 2}(k^*_{(x)})^{2/3}(\rho^*_{(x)}V_{(x)})^{\cdot 8}[(1-\sqrt[3]{p^*_r}h_{(x)} + \sqrt[3]{p^*_r}h_{(0)} - h_{(w)}]}{(\mu^*_{(x)})^{7/15}(C^*_{P(0)})^{2/3}x^{\cdot 2}} \quad (20)$$

Using Reynolds analogy, the laminar and turbulent shear stress and friction coefficients are calculated from:

$$C_{f_{Lam}} = \frac{2\dot{q}_{Lam}(p^*_{r(x)})^{2/3}}{\rho_{(x)}V_{(x)}(h_{rec} - h_{(w)})g} \quad (21)$$

$$C_{f_{Turb}} = \frac{2\dot{q}_{Turb}(p^*_{r(x)})^{2/3}}{\rho_{(x)}V_{(x)}(h_{rec} - h_{(w)})g} \quad (22)$$

$$\tau_{Lam} = 0.5\,C_{f_{Lam}}\,\rho_{(x)}\,V^2_{(x)} \quad (23)$$

$$\tau_{Turb} = 0.5\,C_{f_{Turb}}\,\rho_{(x)}\,V^2_{(x)} \quad (24)$$

The local Reynolds number is calculated from

$$R_{e(x)} = \frac{\rho_{(x)}V_{(x)}X}{\mu_{(x)}} \quad (25)$$

and the momentum thickness Reynolds number is (see Reference 2)

$$Re_{(\theta)} = \frac{0.87\,f''_{(w)}\,\rho_{(w)}\,\mu_{(w)}}{C_{f(w)}\,\rho_{(x)}\,\mu_{(x)}} \quad (26)$$

in which the Cohen and Reshotko's (Reference 7) velocity gradient parameter, $f''_{(w)}$, is curve fitted by the following two equations (valid for favorable pressure gradients):

(a) $C_f\,R_e/N_u > 2$

$$(27)$$

$$f''_{(w)} = 0.0508\,[C_f\,R_e/N_u]^2 + 0.1332\,[C_f\,R_e/N_u]$$

4

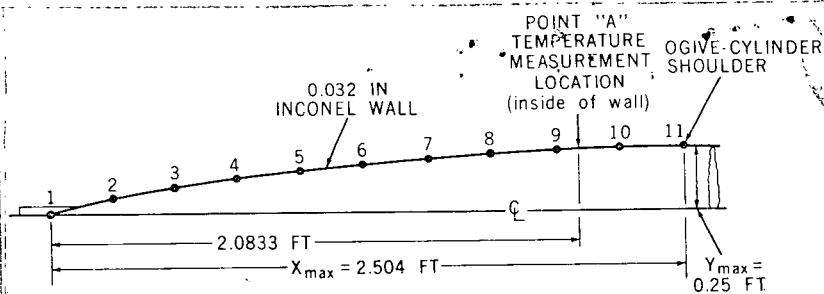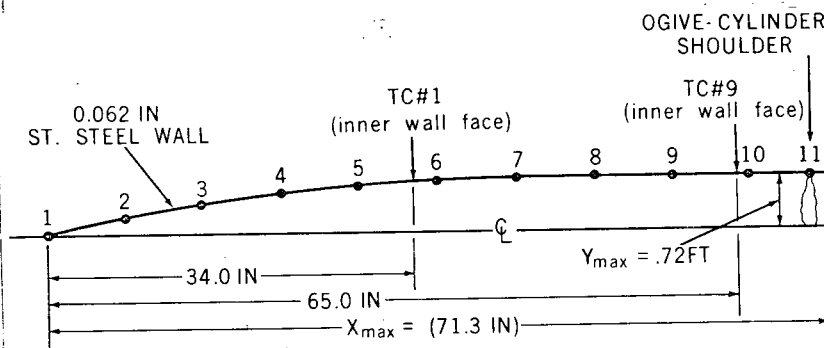Figure 3A. Sketch of the vehicle Nose for NASA TND889

Figure 3B. Sketch of Black Brant VC Nose Showing Locations of Thermocouples

(b) $0 \le C_f \cdot R_e / N_u \le 2$

$$\text{(28)}$$

$$f''_{(w)} = 0.011627 \, [C_f \, R_e / N_u]^2 + 0.25644 \, [C_f \, R_e / N_u] - 0.089787$$

Shock and Expansion Routines

The real gas oblique shock routine for hypersonic flow and the method of accounting for the pressure and entropy gradients across the shock layer for conical flow are given in Appendix B of Reference (3). This hypersonic analysis (real gas in equilibrium) becomes invalid in the medium to low supersonic range so an alternate supersonic conical shock calculation method (perfect gas see Appendix C of Reference 3) is available upon failure of the hypersonic analysis.

Similarly, a real gas (applicable for hypersonic Mach number ranges) Prandtl-Meyer expansion routine (Figure
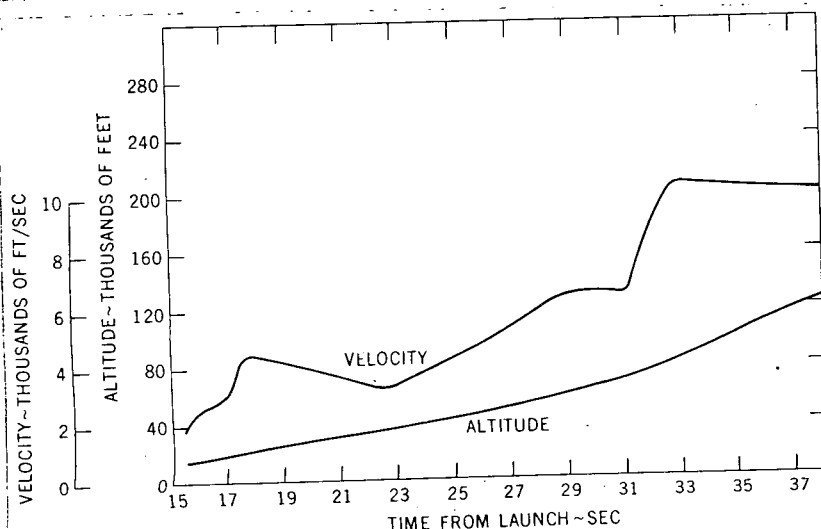

Figure 4. Velocity and Altitude Histories for the Flight of the Vehicle of Figure 3A through the Significant Aeroheating Portion of Flight

4, Reference 2) is valid only down to local Mach numbers somewhere between 2 and 3. As with the cone shock calculations, the real gas Prandtl-Meyer analysis is backed up by a perfect gas routine (Appendix D, Reference 3) which is used when failure of the real gas method occurs. Note that in either the shock or expansion analysis for low supersonic flow, the perfect gas assumption is quite valid.

Cross Flow Corrections

The derivation of the effects of cross flow on a cone at moderate angle-of-attack is taken from the work of J. Sternberg and is given in some detail in Reference (3). The resulting equations are:

$$QRATL = \left[\frac{\dot{q}_{with\ cross\ flow}}{\dot{q}_{without\ crossflow}} \right]_{Laminar} \tag{29}$$

$$= \left[\frac{1 + \dfrac{2\,Tan\,(\theta_c + \alpha)}{Tan\,\theta_c}}{3} \right]^{1/2}$$

and

$$QRATT = \left[\frac{\dot{q}_{with\ cross\ flow}}{\dot{q}_{without\ cross\ flow}} \right]_{Turbulent} \tag{30}$$

$$= 0.85\,(1 + k_2)^{.2}$$

where

$$k_2 = 1.25 \left[\frac{Tan\,(\theta_c + \alpha)}{Tan\,\theta_c} \right]$$

These equations are used to estimate the effects of cross flow on the ogive nose. Both equations are solved at each station on the ogive assuming the local surface angle, θ, to be the "cone half-angle," θ_c. Note that when the angle-of-attack, α, goes to zero, both QRATL and QRATT go to one. Finally, it must be remembered that even when properly used (for cone flow) Equations (29) and (30) are valid only for $(\theta_c + \alpha)$ values up to approximately 35 degrees. As the deflection angle plus angle-of-attack exceeds this range, the cross flow begins to dominate the aeroheating phenomenon and a better analytical prediction derives from a two-dimensional, blunt body method like that of Reference (2). Obviously, the crossover point for the applicability of either theory is not clearly defined.

Hemi-Spherical Nose Stagnation Heating

There are two reasons for including the calculation of the hemi-spherical nose calculation in this analysis. First, the post-normal shock flow properties are required for the laminar boundary layer heat rate calculation of Equation (13) and, in the same equation, the stagnation heat rate is specifically required to redimensionalize the heat ratio to get the absolute value of the local laminar heat rate. The second reason lies in the fact that the stagnation point heat transfer is often desired as a general heat transfer parameter for evaluating the effects of trajectory parameters, vehicle weight, etc., upon the vehicle thermal environment.

Note that the nose radius selected for the calculation enters into the solution of Equation (13) only via the $H^*_{(0)}$ term (Equation 18) in the form of the stagnation point velocity gradient (Equation 19). The same nose radius is also used in the stagnation point heating rate (Equation 31) so it is clear that all data relative to body points 1 through 15 are totally independent of the value of RN. For this reason it is suggested that a value of RN = 1 foot be assumed because this is commonly used as a heat indicator.

The stagnation point heat rate can be calculated by the equation of Fay and Riddell (Reference 8) with the Lewis number assumed equal to unity:

$$\dot{q}_{stag.\,point} = 0.76\, g\, (P_r)^{-.6}\, (\rho_{(w)}\, \mu_{(w)})^{.1}\, (\rho_{(x)}\, \mu_{(x)})^{.4}\, (h_{(0)} - h_{(w)}) \left(\frac{dV}{dx}\right)_0^{1/2} \quad (31)$$

Detachment of Nose Shock Wave

The method of estimating the point 1 conditions by assuming the conical nose shock wave that would result from a cone of half-angle equal to the angle shown as $(\theta + \alpha)$ in Figure 2 does introduce a possible problem. If $(\theta + \alpha)$ at any given free stream Mach number is greater than some critical flow deflection angle, δ_{cr}, the nose shock will detach and the analytical methods will become invalid. In order to protect against this possibility (which can arise from either too blunt an ogive, too large an angle-of-attack, or a combination of the two), the critical conical flow deflection angle as a function of free stream Mach number is taken from chart 5 of Reference (9). Thus, for each problem, the nose apex flow deflection angle (including angle-of-attack) and the free stream Mach number are known. The analyst uses the free stream Mach number in the appropriate region of Figure 5 (Reference 9) to obtain the maximum allowable flow deflection angle, δ_{cr}. This angle is then compared with the actual deflection angle $(\theta + \alpha)$ at the nose and if $\delta_{cr} < (\theta + \alpha)$, it is clear that the shock is detached and the present analysis is inapplicable.

Comparison of Theory With Flight Data

In order to test the theory presented here with flight data, two cases are considered: a four stage vehicle reported in Reference (11) and Black Brant VC, Flight 21.006 UG (Reference 10).
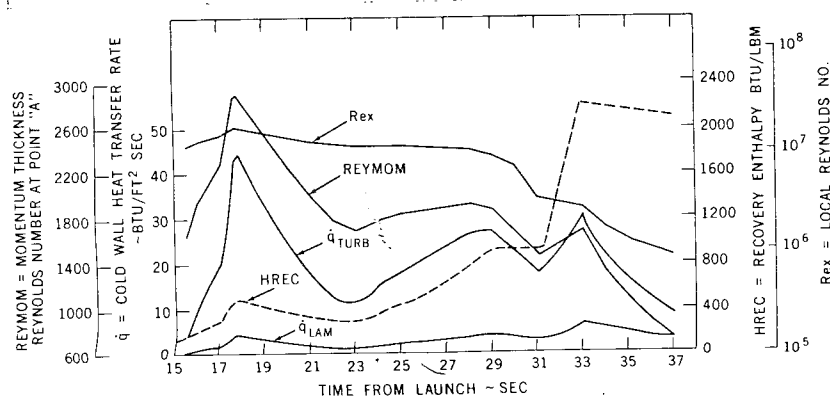

Figure 5. Laminar and Turbulent Heat Transfer Rates, Recovery Enthalpy, Local Reynolds Number and Momentum Thickness Numbers at Point "A"

I. Comparison With Flight Data From NASA TND 889 (Reference 11)

The vehicle nose of Figure 3A was flown on a four stage vehicle with a temperature history measured on the inside of the 0.032 inch inconel wall at the position marked "point A" on the sketch. The velocity and altitude histories of the test vehicle through the significant heating portion of flight (during which valid temperature data were recorded) are shown in Figure 4. Using these trajectory data and the nose configuration of Figure 3A, the laminar and turbulent heat rate, recovery enthalpy, and the local Reynolds number data of Figure 5 were calculated by the methods of this paper (using the computer program NQL-DW019 from Reference 1). The Prandtl-Meyer expansion method of obtaining local pressures was used.

These data were then input to a 10-element, one-dimensional structural heating program (NQLDW112, Reference 12) to obtain the temperature histories shown as solid lines in Figure 6. Note that the cases of a fully turbulent boundary layer and of transition at local Reynolds numbers of 2.8, 5.0 and 10.0 million are presented. The flight recorded temperature data are shown as circled points.

In general, the agreement between theory and flight data is quite good. The data indicate that transition from turbulent to laminar flow probably occurred at a calculated local Reynolds number of seven to eight million. It is emphasized that this local Reynolds number is defined as:

$$Re_{x_{(Tr)}} = \frac{\rho_{(x)}\, V_{(x)}\, X}{\mu_{(x)}} \quad (32)$$

where the sub x values are taken at the outer edge of the boundary layer at point A. Inasmuch as the manner of approximating the effects of the entropy gradient through the shock layer results in more or less fictitious values of the local entropy at any given point, caution must be used in comparing the transition Reynolds number as defined by Equation (32) with transition Reynolds numbers from other sources which do not make the same local entropy value assumptions.

II. Comparison With Flight Data From Black Brant VC Flight 21.006 GT (Reference 10)

The vehicle nose of Figure 3B was flown on Flight 21.006 GT, a Black Brant VC, and two thermocouples were located on the inner surface of the 0.062 inch stainless steel wall at the positions indicated as TC #1 and TC #9 in the sketch. The trajectory used in the calculations is taken from radar data and the velocity and altitude histories are shown in Figure 7. The digital program (NQLDW019) was used to derive the heat transfer rate data of Figures 8 and 9 for TC #1 and TC #9, respectively. These data, again using the structural heating analysis of Reference (12), result in the temperature predictions (solid lines) of Figures 10 and 11.

If transition from turbulent to laminar flow is assumed to occur at a local Reynolds of ten million at TC #1, the agreement between theory and flight is seen
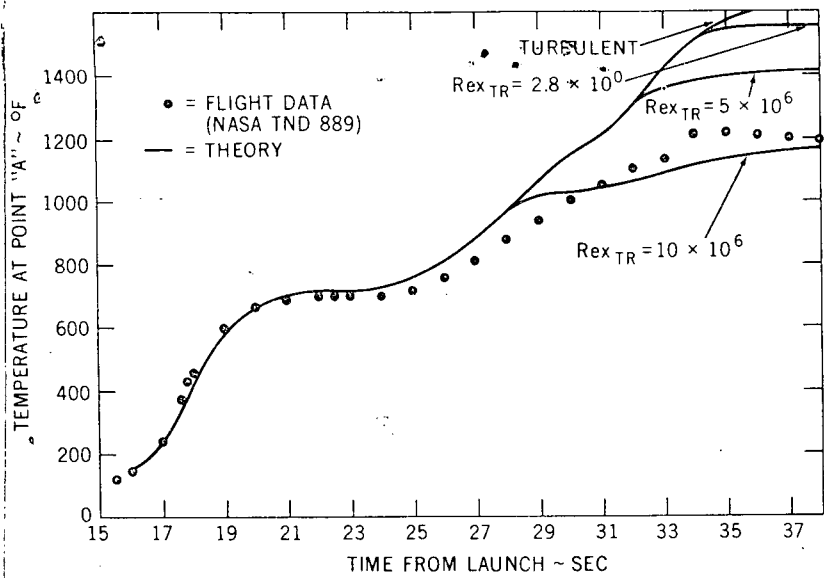
Figure 6. Comparison of Flight with Theoretical Data Using the Theory of NQLDW019 to Predict the Heat Rate History
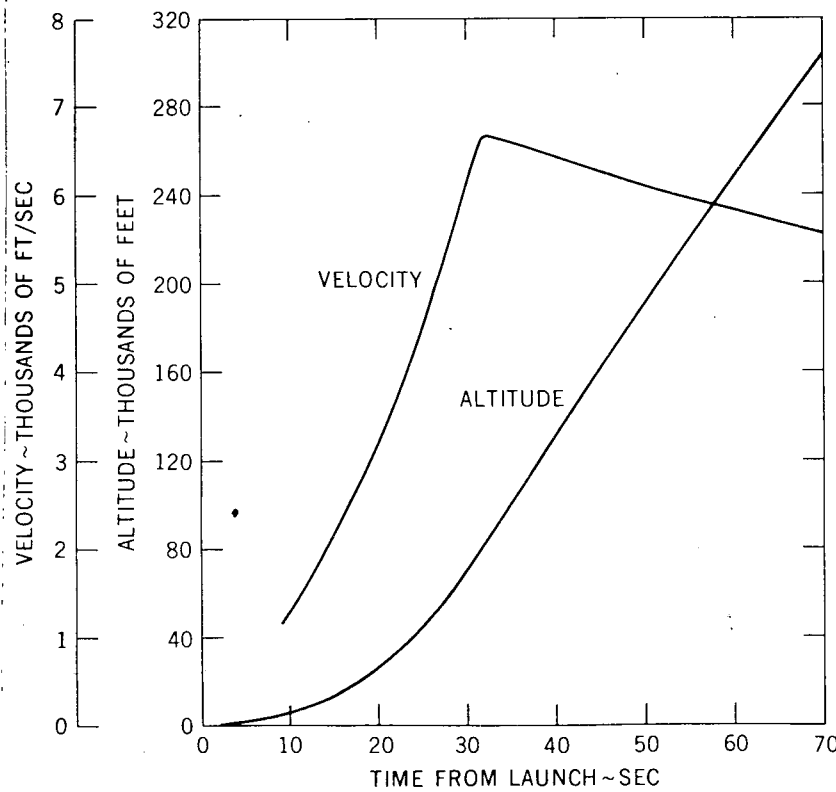

Figure 7. Black Brant VC Flight 21.006GT Ascent Radar Trajectory Data

Figure 8. Black Brant VC Flight 21.006GT Heat Transfer Rate at TC1
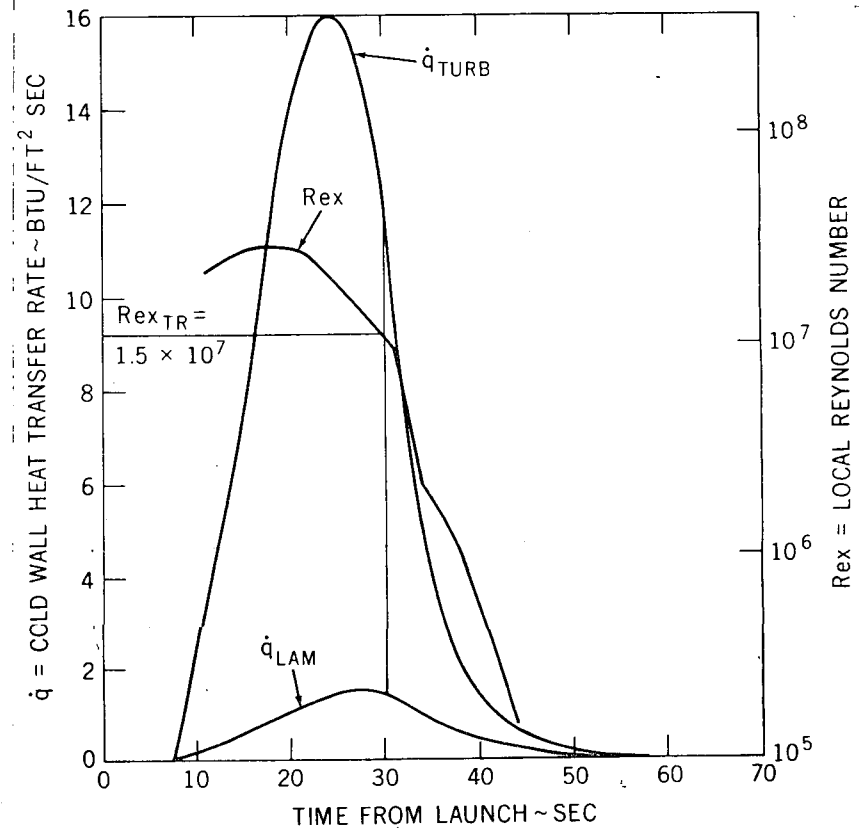
Figure 9. Black Brant VC Flight 21.006GT Heat Transfer Rate at TC9

(Figure 10) to be extremely good. Similarly, the assumption of a transition Reynolds number of 15 million at TC #9 results in good agreement between theory and measurement.

Transition Reynolds Number

It certainly comes as no surprise that the ability to predict the heat transfer rate is primarily dependent upon the ability to predict the nature of the local boundary layer. This holds true whether the analytic approach be approximate (as in the present case) or involves a complete numerical solution of the boundary layer equations. Figures 6, 10 and 11 indicate that the present analysis is adequate if the transition can be predicted. Accordingly, an empirical method for predicting the transition Reynolds number is sought by the simple expedient of recording experimental values as they are inferred by
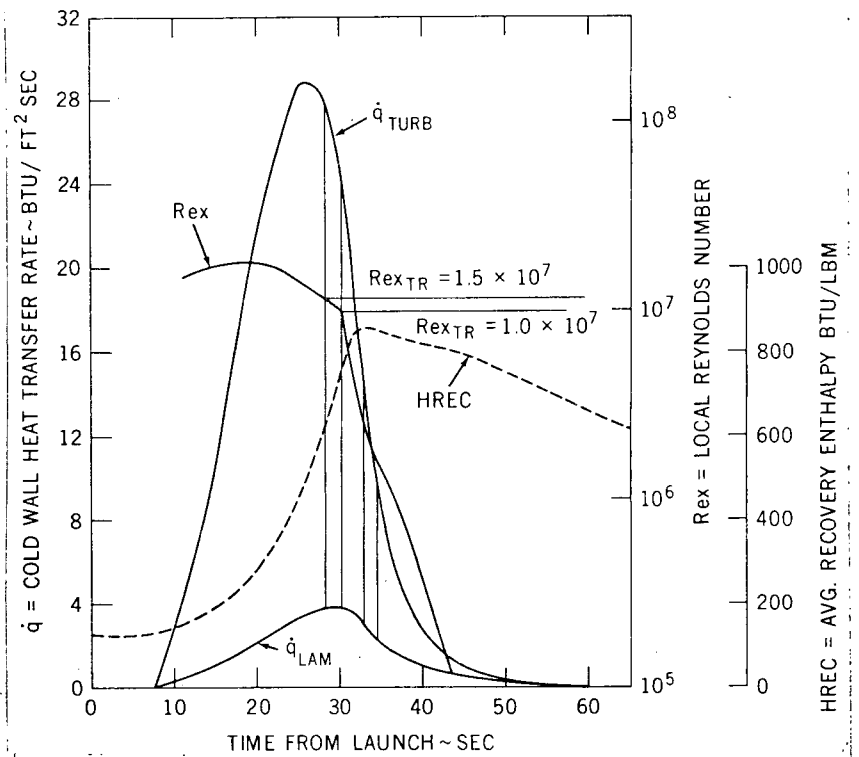
comparison of the heating analysis predictions with the flight temperature data as has just been demonstrated.

Such a comparison is shown in Figure 12. Of course, with the scant amount of data available the ability to predict transition Reynolds numbers for all tangent ogives at all flight conditions is almost totally absent. On the other hand, it should be borne in mind that the flight regimes, degrees of bluntness of the ogives and general body surface conditions for large families of sounding rockets are sufficiently restricted as to make such an empirical approach quite practicable. In the present case (Figure 12), only thin-wall, metallic ogives are represented.
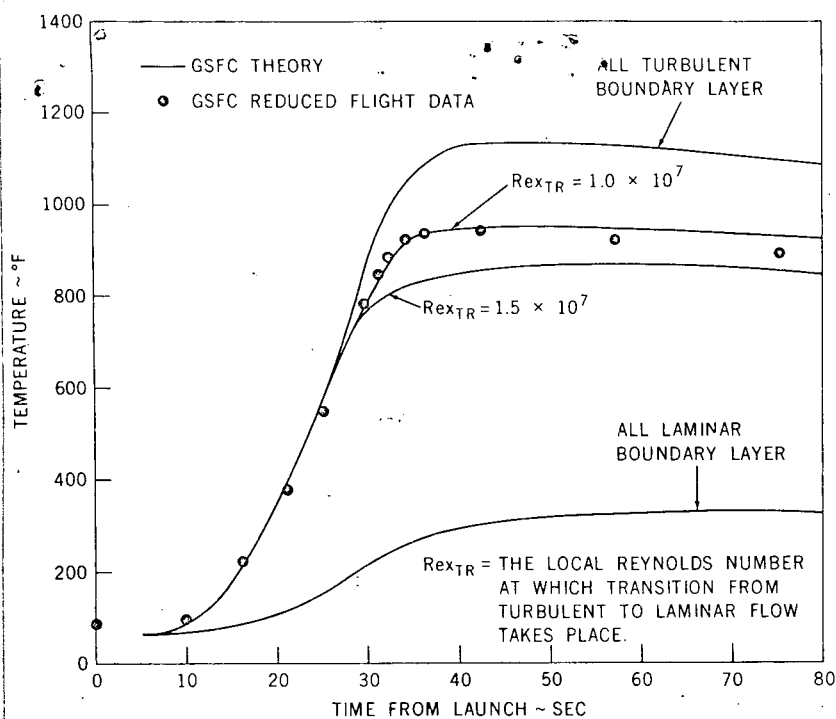
7

Figure 10. Black Brant VC Flight 21.006GT Temperature of 0.062" Stainless Steel Wall at TC1
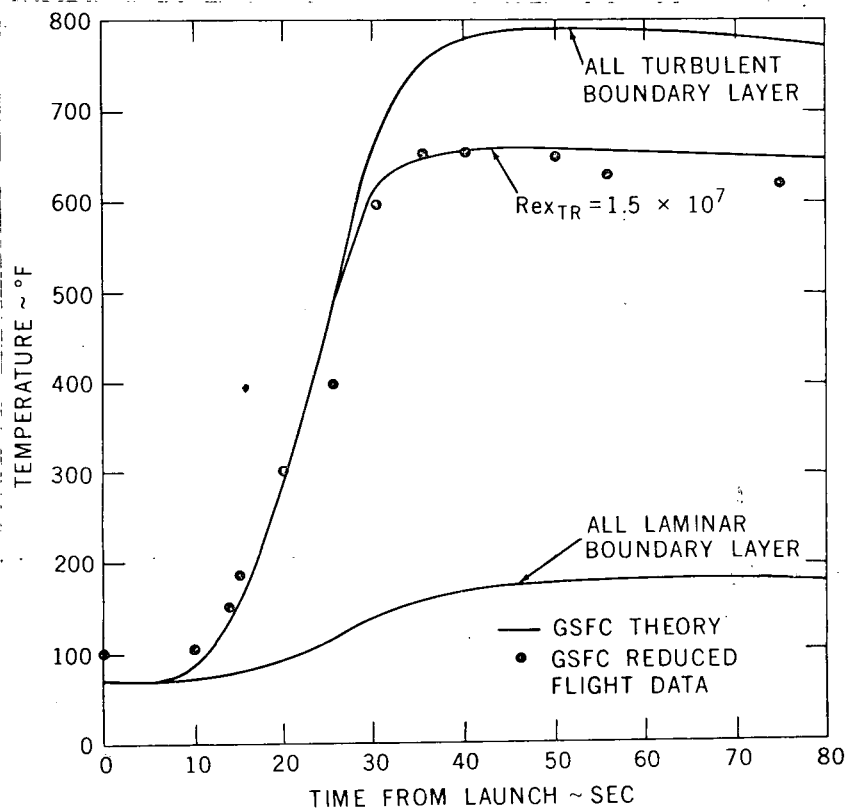

Figure 11. Black Brant VC Flight 21.006GT Temperature of 0.062" Stainless Steel Wall at TC9

It is quite likely that low conductivity noses (i.e., fiberglass phenolic) would have appreciably different ratios of external surface to local recovery temperatures and thence would be expected to require a separate curve such as that of Figure 12. Over a period of time, then, the use of the present theory should reasonably quickly allow an investigator to attain an adequate ability to predict the effects of aerodynamic heating on any tangent ogive nose.

Conclusions

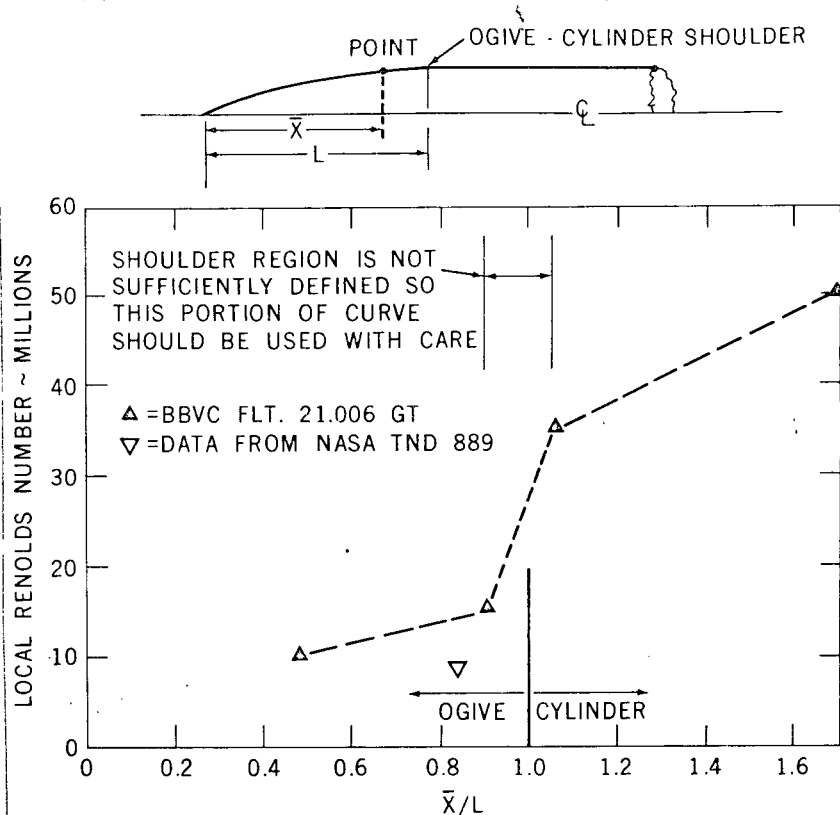The following conclusions are drawn from the work reported:

Figure 12. Summary of Transition Local Reynolds Number Which Best Matches Flight Temperatures with Present Theoretical Predictions vs Ratio of Point Location on Centerline to Centerline of Ogive from Two Flights

1. The tangent ogive aeroheating analysis methods described are capable of providing adequate predictions of the aerothermal effects on tangent ogive noses of typical sounding rockets.

2. The accuracy with which these predictions can be made is dependent primarily upon the accuracy with which transition from turbulent to laminar flow (in ascent) or laminar to turbulent flow (in re-entry) can be predicted. The extreme complexity of the boundary layer transition phenomenon suggests that the empirical approach is the most practical at this time, particularly when large numbers of similar vehicles are involved as is often the case with sounding rockets.

3. Only a relatively small amount of data for checking the validity of the conical cross flow analysis (incorporated in the present method by the assumption of local similarity) has been obtained to date so caution is advised in its use until further corroboration is available.

References

1. "Tangent Ogive Nose Aerodynamic Heating Program: NQLDW019" by L. D. Wing, NASA Goddard Space Flight Center Document X-742-71-161, April 1971

2. "Digital Utilization Program FM147—General Aerodynamic Heating" by L. D. Wing, Report No. ER-109, October 1967, Technical Services Division, Fairchild Hiller Corporation

3. "Aerodynamic Heating for Wedge/Wedge or Cone/Cone at Angles-of-Attack from Zero to Approximately 40°" by L. D. Wing, Report No. ER-116, November 1968, Technical Services Division, Fairchild Hiller Corporation

8

4. "Approximations for the Thermodynamic and Transport Properties of High Temperature Air" by C. F. Hansen, NASA Technical Report R-50, 1959

5. "Use of Reference Enthalpy in Specifying the Laminar Heat Transfer Distribution Around Blunt Bodies in Dissociated Air" by E. R. G. Eckert and O. E. Tewfik, Journal of the Aero/Space Sciences, Pg. 464, Vol. 27, No. 6, June 1960

6. "Evaluation of Several Hypersonic Turbulent Heat Transfer Analyses by Comparison with Experimental Data" by P. A. Libby and R. J. Cresci, WADC Technical Note 57-72, July 1957, ASTIA DOC. NO. AD 118093

7. "Similar Solutions for the Compressible Laminar Boundary Layer with Heat Transfer and Pressure Gradient" by C. B. Cohen and E. Reshotko, NACA Report 1293, 1956

8. "Theory of Stagnation Point Heat Transfer in Dissociated Air" by J. A. Fay and F. R. Riddell, Journal of the Aero/Space Sciences, Pg. 73, Vol. 25, No. 2, February 1958

9. "Equations, Tables, and Charts for Compressible Flow," NASA Ames Research Staff, NACA Report 1135, 1953

10. "Comparison of Analytical Temperature Predictions With Flight Data for Black Brant VC (BBVC) Flight 21.006GT", U. S. Government Memorandum from Mr. L. D. Wing to Analysis Section Files dated 17 March 1972

11. "Free Flight Aerodynamic Heating Data to Mach Number 10.4 for a Modified Von Karman Nose Shape" by Wm. M. Bland, Jr. and K. A. Collie, NASA TND 889, May 1961

12. "10 Element One-Dimensional Structural Heating Programs" by L. D. Wing, NASA Goddard Space Flight Center Document X-721-69-454, August 1969